Journal of Research in Science and Engineering (JRSE)
ISSN: 1656-1996 Volume-8, Issue-3, March 2026
DOI: 10.53469/jrse.2026.08(03).03

Thermal Flow Field Analysis and Structural Optimisation of The Stretching Oven for PP Strapping Tape

Shubing Zhou, Zhewei Ye*

School of Mechatronic Engineering, Southwest Petroleum University, Chengdu 610500, Sichuan, China
**Correspondence Author*

Abstract: ***As the core preheating equipment in polypropylene (PP) strapping tape production, the stretching oven's performance is critically influenced by the uniformity of its internal thermal flow field, which directly determines the molecular chain orientation of the tape blank and the final product's mechanical properties. Addressing prevalent operational issues such as non-uniform temperature distribution, localized eddy currents causing excessive temperature gradients across the tape blank, and significant fluctuations in final product thickness, this study focuses on a double-belt PP strapping tape stretching oven. A three-dimensional geometric model was constructed using SolidWorks, and computational fluid dynamics (CFD) simulations were performed with its Flow Simulation module. The analysis employed the standard k-ε turbulence model to investigate the distributions of temperature and velocity fields within the oven systematically. The reliability of the numerical model was validated through experiments involving platinum resistance thermometry and hot-wire anemometry, with a maximum relative error of ≤10%. Four distinct structural optimization schemes were subsequently designed and compared. Results indicated that the original oven configuration yielded a maximum temperature difference of 1.5 °C and a relative RMS deviation of velocity of 0.54 in the strapping tape channel, corresponding to product width fluctuations of ± 0.3 mm. Among the proposed modifications, Optimization Scheme 1, which incorporated curved spacers within the air ducts, demonstrated the most significant improvement. This design reduced the maximum temperature difference to 1.0 °C and decreased the velocity's relative RMS deviation to 0.25—a reduction of 53.7%. Consequently, the product width fluctuation range was narrowed to ± 0.2 mm, representing a 33.3% improvement in dimensional consistency. This research provides a theoretical foundation and practical guidance for enhancing the performance of strapping tape stretching ovens.***

Keywords: Strapping Tape stretching oven, Thermal flow field uniformity, CFD simulation, Structural optimisation**.**

1. Introduction

Polypropylene (PP) strapping tape, an environmentally friendly packaging material, is widely used in logistics bundling and industrial packaging owing to its high strength, low weight, and recyclability. The stretching process is a critical stage in strapping tape production, during which the strapping tape blank is preheated in a stretching oven to near the material's glass transition temperature (approximately 120–140 °C for PP). This heating facilitates the alignment of molecular chains during subsequent directional stretching, thereby enhancing the product's tensile strength and toughness. Research by Zhang et al. [1] on various stretching processes demonstrated that for oriented polypropylene sheets, the crystalline structure and molecular orientation improve progressively with increasing temperature up to 142 °C, resulting in higher tensile strength. Consequently, the uniformity of the thermal flow field within the oven is paramount, as it governs the temperature consistency of the strapping tape blank, which directly dictates the degree of molecular chain orientation and the final mechanical properties of the strapping tape.

Currently, many stretching ovens employ a conventional layout comprising axial fans, heating pipes, and straight air ducts. Suboptimal duct design within this configuration often leads to operational issues such as airflow maldistribution, localised eddy currents, and stagnant flow zones. While extensive research has been conducted on improving thermal uniformity in drying equipment and general-purpose ovens, focused studies on strapping tape stretching ovens remainlimited. Pertinent optimisation strategies documented in related fields include: Shi Jianfang et al. [2] using CFD simulation to enhance material temperature uniformity by redesigning the air inlet of a tunnel drying kiln; Bedelean [3] demonstrating that incorporating a top baffle yields a more rational airflow distribution within a kiln; and Sjövall F et al. [4] proposing a topology optimisation method, offering a novel approach for designing internal ducts in heat exchange equipment. Within packaging machinery specifically, Amjad et al. [5] improved dryer airflow distribution via diagonal inlet channels, while Lin Zhe et al. [6] applied hydrodynamic principles to optimise a packaging valve flow field, achieving a 52% improvement in flow accuracy. The methodologies and outcomes from these studies provide a valuable foundation for optimising the thermal flow field in strapping tape stretching ovens.

Nevertheless, a paucity of dedicated research persists for strapping tape stretching ovens. Notably, advanced methodologies such as data-driven optimisation and coupled radiation-convection simulations, increasingly prevalent in recent years, have seen limited application to this specific equipment type. To address this gap, the present study employs SolidWorks Flow Simulation to implement a comprehensive workflow encompassing geometric modelling, numerical simulation, experimental validation, and structural optimisation. A targeted design modification scheme is proposed and its efficacy rigorously evaluated through experimental testing. This work aims to furnish both technical underpinnings and practical solutions for advancing the production equipment of strapping tape towards higher precision standards.

2. Simulation of the Thermal Flow Field in the Stretching Oven

2.1 Physical Model and Mesh Generation

2.1.1 Three-Dimensional Modelling

A three-dimensional model of the stretching oven was developed in SolidWorks, based on the specifications of a commercial PP lightweight strapping production line. The overall equipment dimensions are 4000 mm (L) × 860 mm (W) × 1760 mm (H). As illustrated in Figure 1, the primary components include centrifugal fans, fan ducts, a heating chamber, strapping channels, and air outlets/inlets. The core structural parameters are:

Centrifugal fan: power = 0.75 kW, rotational speed = 2800 r/min, air volume flow rate = 1800 m^3/h.

Heating chamber: channel dimensions = 300 mm (W) × 200 mm (H) × 3200 mm (L); contains 14 heating tubes, each rated at 2 kW.

Strapping tape channel: width = 276 mm, height = 485 mm; strapping tape blank travel speed = 30 m/min (for standard operating conditions).

Model Simplification Principles: To focus the computational analysis on the core flow domain, components with negligible influence on the flow field—such as heating pipe terminals and fan motors—were omitted. Furthermore, the surfaces of the strapping tape channel and the heating chamber were modelled as ideally smooth walls. This simplification approach, which reduces geometric complexity while preserving essential physics, is well-established in engineering CFD practice [7]. The resulting simplified computational model is presented in Figure 2.

Figure 1: Physical photograph of the strapping tape stretching oven

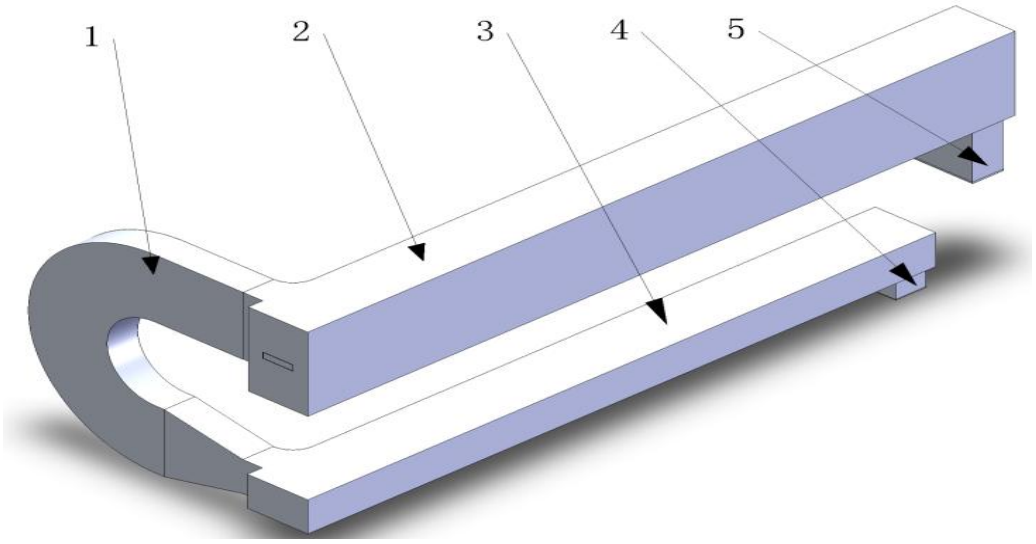

1—Fan duct, 2—Strapping tape channel, 3—Heating chamber, 4—Air inlet, 5—Air outlet

Figure 2: Simplified computational model of the strapping tape stretching oven

2.1.2 Mesh Generation and Grid Independence Study

A hybrid meshing strategy was employed within the SolidWorks Flow Simulation environment. The global mesh was generated with a base size corresponding to a resolution level of 3 (or finer). To accurately capture the thermal gradients in critical regions, local mesh refinement was applied to the heating chamber, increasing the resolution to a

level of 4 or higher [8].

A grid independence study was conducted to ensure that the numerical results were not influenced by mesh density. Four distinct mesh schemes with progressively increasing element counts were created. The area-weighted average temperature at the outlet plane was selected as the monitoring parameter. The results of this study, demonstrating the convergence of the solution with increasing mesh density, are summarised in Table 1.

Table 1: Results of the grid independence study.

No	Gridnumber/$\times 10^6$	Outlet Temperature/°C
1	1.09	79.65
2	2.83	84.85
3	3.49	83.41
4	6.07	83.4

Based on a balance between computational cost and solution stability, a final mesh comprising approximately 3.49 million elements was selected. The generated computational mesh is displayed in Figure 3.

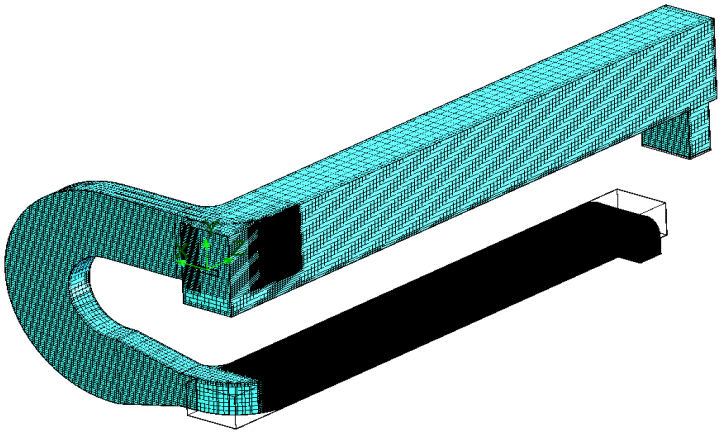

Figure 3: Calculation grid of strapping tape stretching oven

2.2 Mathematical Model

The coupled airflow and heat transfer processes within the oven are governed by the following set of equations:

(1) Turbulence model

Based on the flow characteristics within the oven, the standard k-ε turbulence model was employed for the simulations [9]. The dissipation rate ε is

$$\varepsilon = \frac{\mu}{\rho}\left(\frac{\partial u_i}{\partial x_k}\right)\left(\frac{\partial u_i}{\partial x_k}\right) \quad (1)$$

where ε is the dissipation rate, μ is the dynamic viscosity coefficient (N.s/m^2) , ρ is the fluid density (kg/m^3), u_i is the velocity (m/s) in the i (x, y or z) direction, and x_k is the displacement (m) in the k direction.

The turbulent viscosity μ_t is

$$\mu_t = \rho C_\mu \frac{k^2}{\varepsilon} \quad (2)$$

where C_μ is an empirical constant, which takes the value of 0.09 in flow simulation.

In the standard k-ε model, k and ε are the two basic unknowns, and the equation is

$$\frac{\partial(\rho k)}{\partial t} + \frac{\partial(\rho k u_i)}{\partial x_j} = \frac{\partial}{\partial x_j}\left[\mu + \frac{\mu_t}{\sigma_k}\frac{\partial k}{\partial x_j}\right] + G_k + G_b - \rho\varepsilon - Y_M + S_k \quad (3)$$

$$\frac{\partial(\rho\varepsilon)}{\partial t} + \frac{\partial(\rho\varepsilon u_i)}{\partial x_i} = \frac{\partial}{\partial x_j}\left[\left(u + \frac{\mu_t}{\sigma_\varepsilon}\right)\frac{\partial \varepsilon}{\partial x_j}\right] + C_{1\varepsilon}\frac{\varepsilon}{k}(G_k + C_3\varepsilon G_b) - C_{2\varepsilon}\rho\frac{\varepsilon^2}{k} + S_\varepsilon \quad (4)$$

Where:

G_k represents the generation of k due to the mean velocity gradients;

G_b is the generation of k due to buoyancy;

Y_M represents the contribution of fluctuating dilatation to the overall dissipation rate in compressible turbulence;

$C_{1\varepsilon}$, $C_{2\varepsilon}$ and $C_{3\varepsilon}$ are the empirical constants;

x_i, x_j are the displacements (m) in the direction of i, j;

σ_k, σ_ε are the turbulent Prandtl numbers for k and ε, respectively;

S_k and S_ε are user-defined source terms.

(2) Continuity equation

According to the law of conservation of mass, the total net mass outflow from the control volume per unit time is equal to the mass inflow from the outside into the control body in the same time, i.e.

$$\frac{\partial \rho}{\partial t} + \frac{\partial(\rho u_x)}{\partial x} + \frac{\partial(\rho u_y)}{\partial y} + \frac{\partial(\rho u_z)}{\partial z} = 0 \quad (5)$$

Where:

t is the time (s);

u_x, u_y, u_z is the flow velocity (m/s) of the fluid in the x, y, z direction respectively.

(3) Momentum equation

The sum of the external forces acting on the microelement body is equal to the rate of change of the fluid momentum in

the microelement body against time. Fluid in the x, y, z three directions on the momentum conservation equation is expressed in the form of

$$\frac{\partial(\rho u)}{\partial t} + \mathrm{div}(\rho u u) = \mathrm{div}(u\,\mathrm{grad}u) - \frac{\partial p}{\partial x} + S_u \quad (6)$$

$$\frac{\partial(\rho v)}{\partial t} + \mathrm{div}(\rho v \vec{u}) = \mathrm{div}(\mu\,\mathrm{grad}v) - \frac{\partial p}{\partial y} + S_v \quad (7)$$

$$\frac{\partial(\rho w)}{\partial t} + \mathrm{div}(\rho w \vec{u}) = \mathrm{div}(\mu\,\mathrm{grad}w) - \frac{\partial p}{\partial z} + S_w \quad (8)$$

Where:

μ is the velocity vector (m/s);

p is the pressure (N) on the fluid micrometabolite;

S_u, S_v, S_w are generalised source terms.

2.3 Boundary Conditions and Solver Settings

Within the SolidWorks Flow Simulation framework and in accordance with thermodynamic and fluid dynamic principles, the following boundary conditions were configured to model the oven start-up condition [8]:

Inlet: Defined as a mass flow inlet, with specified volumetric flow rate and temperature. The flow was assumed to be fully developed.

Walls: The external walls were set as adiabatic. A no-slip condition was applied at all fluid-solid interfaces.

Outlet: Set as a pressure outlet, corresponding to natural outflow at ambient atmospheric pressure.

The specific parameters are listed in Table 2.

Table 2: Setting conditions of simulation

Parameter	Value
Material of stretching oven	Material of stretching oven
Material of fluid	Air
Inlet volume flow rate/(m^3/s)	0.5
Inlet Temperature/°C	17.8
Fully Developedflow	Surface Heat Generation Rate/(W/m^2)
Surface Heat Generation Rate/(W/m^2)	11446
Convergence Criterion/°C	1

2.4 Model Validation

2.4.1 Experimental setup

An experimental platform was established to characterise the thermal flow field within the oven. Given that the oven's operating temperature exceeds the measurement range of the hot-wire anemometer, temperature and velocity measurements were conducted separately. Velocity measurements were performed with the heating system deactivated. Temperature distribution was measured using Pt100 platinum resistance temperature sensors (accuracy: ±0.1 °C). Air velocity was measured with a DT-3880 hot-wire anemometer (accuracy: ±5.0% ±0.03 m/s). The sensors were arranged in a three-dimensional 3×3×3 matrix within the strapping tape channel's working zone. This matrix comprised upper, middle, and lower layers. Within each layer, nine measurement points were located at the intersections of three front-to-back positions and three left-to-right positions. The vertical spacing between the middle and lower layers was 200 mm. Horizontally, the spacing between adjacent front-to-back points was 100 mm, and the spacing between adjacent left-to-right points was 1000 mm. The layout of the measurement points is illustrated in Figure 4.

2.4.2 Verification results

Experiments were conducted under two distinct operating conditions: (1) with the heating system deactivated while the fan operated at its rated speed, and (2) with the oven heating temperature set to 100 °C and the air outlet disconnected. A comparison between the simulated and corresponding measured data is presented in Table 3. The results indicated that the relative errors in temperature across all 27 measurement points ranged from 1.31% to 3.21%, yielding a mean relative error of 2.12%. For the average air velocity, the relative errors ranged from -3.05% to -9.84%, with a mean of -5.57%. The observed discrepancies are attributed primarily to sensor installation uncertainties and the inherent simplifications of the numerical model. As all error margins fall within the accepted tolerance for engineering simulations (≤10%), the reliability of the developed computational model is validated.

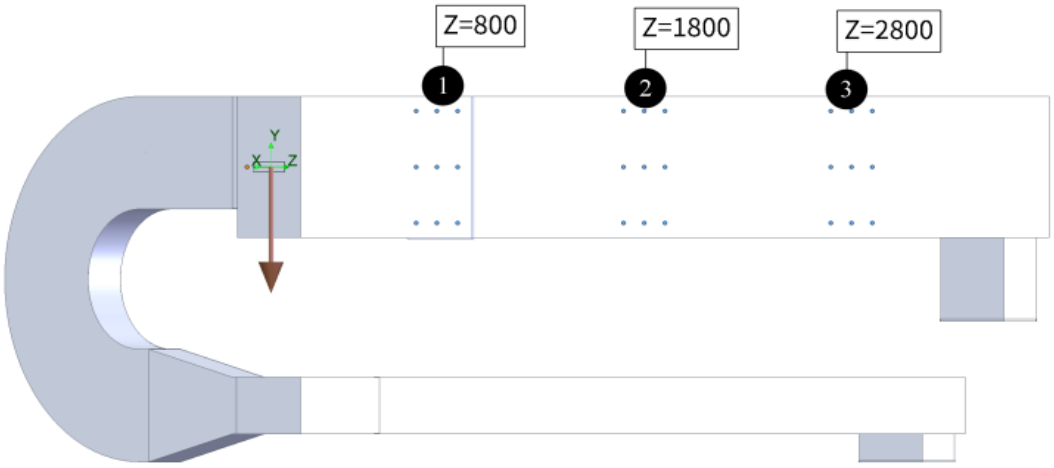

Figure 4: Layout of Measurement Points within the Stretching Oven

Table 3: Comparison of simulated and measured temperature and velocity data.

No.	Coordinate			Temperature (℃)			Wind velocity (m/s)		
	X (mm)	Y (mm)	Z (mm)	Simulated	Measured	Relative Error	Simulation	Measured	Relative Error
1	100	200	800	65.7	67.5	2.77%	1.94	1.77	-8.67%
2	0	200	800	65.7	67.4	2.60%	5.91	5.45	-7.80%
3	-100	200	800	65.7	67.5	2.74%	7.15	6.61	-7.51%
4	100	0	800	65.7	67.6	2.97%	1.85	1.76	-4.66%
5	0	0	800	65.7	67.8	3.21%	1.93	1.74	-9.84%
6	-100	0	800	65.7	67.5	2.72%	7.04	6.78	-3.62%
7	100	-200	800	65.7	67.1	2.19%	0.94	0.89	-4.81%
8	0	-200	800	65.7	67.1	2.16%	2.39	2.28	-4.44%
9	-100	-200	800	65.7	67.2	2.31%	5.22	5.06	-3.05%
10	100	200	1800	65.7	67.3	2.51%	3.60	3.34	-7.14%
11	0	200	1800	65.7	67.2	2.35%	4.46	4.3	-3.59%
12	-100	200	1800	65.7	67.3	2.51%	5.64	5.45	-3.42%
13	100	0	1800	65.7	67.2	2.36%	0.88	0.83	-5.14%
14	0	0	1800	65.7	67.1	2.21%	1.62	1.53	-5.38%
15	-100	0	1800	65.7	67.0	2.06%	3.54	3.41	-3.78%
16	100	-200	1800	65.7	66.8	1.75%	2.61	2.41	-7.56%
17	0	-200	1800	65.7	66.9	1.90%	3.55	3.33	-6.20%
18	-100	-200	1800	65.6	66.8	1.77%	4.46	4.32	-3.16%
19	100	200	2800	65.6	66.8	1.78%	3.70	3.51	-5.24%
20	0	200	2800	65.6	66.6	1.46%	3.99	3.76	-5.76%
21	-100	200	2800	65.6	66.7	1.63%	4.69	4.41	-5.87%
22	100	0	2800	65.6	66.6	1.46%	2.10	1.96	-6.44%
23	0	0	2800	65.6	66.8	1.77%	2.12	2.03	-4.25%
24	-100	0	2800	65.6	66.5	1.31%	2.67	2.47	-7.56%
25	100	-200	2800	65.6	66.6	1.46%	3.22	3.06	-4.94%
26	0	-200	2800	65.6	66.7	1.61%	3.34	3.19	-4.52%
27	-100	-200	2800	65.6	66.8	1.77%	3.47	3.26	-5.94%

3. Results and Discussion

3.1 Evaluation Metrics

To quantitatively assess the performance of the oven, the following two metrics were employed:

(1) Temperature uniformity: the maximum temperature difference, $\Delta T_{max} = T_{max} - T_{min}$, was employed as the evaluation metric.

(2) Velocity Distribution Uniformity: The uniformity of the thermal flow field was assessed using the relative root-mean-square (RMS) deviation of velocity, denoted as $\sigma_v = \sqrt{\frac{1}{n}\sum_{i=1}^{n}\left(\frac{v_i - \bar{v}}{\bar{v}}\right)^2}$ [10]. A lower value of σ_v indicates better flow uniformity. In this formulation quantifies the dispersion of the local air velocity σ_v relative to the cross-sectional mean velocity $\bar{v}$; thus, a higher σ_v corresponds to poorer airflow uniformity. The variable n represents the total number of measurement points on the cross-section, which was 27 in this study.

3.2 Analysis of Thermal Flow Field of the Original Oven Structure

The simulated thermal and flow fields for the baseline oven design are depicted in Figures 5 and 6, respectively. The numerical results at the 27 sensor locations are summarised alongside experimental data in Table 4.

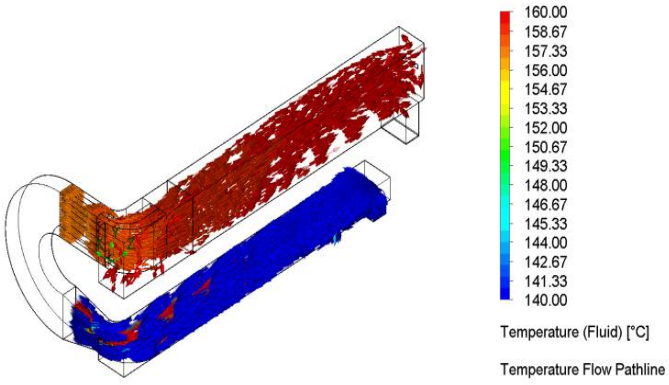

Figure 5: Temperature trace of stretching oven

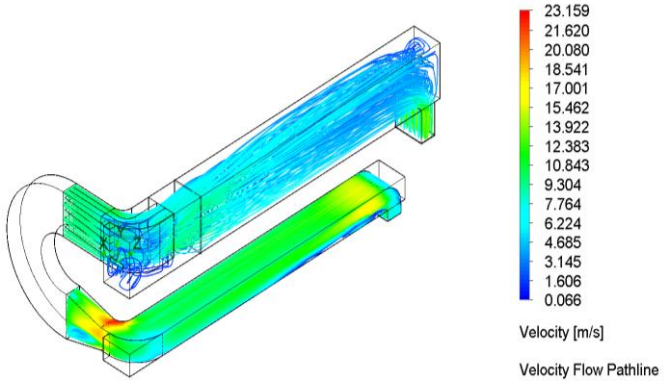

Figure 6: Velocity trace of stretching oven

Table 4: Simulated temperature and velocity data of the original oven

NO.	Coordinate			Temperature (℃)	Wind velocity (m/s)
	X (mm)	Y (mm)	Z (mm)		
1	100	200	800	159.1	2.87
2	0	200	800	158.8	7.21
3	-100	200	800	158.7	9.11
4	100	0	800	159.4	2.53
5	0	0	800	159.1	2.13
6	-100	0	800	158.7	9.20
7	100	-200	800	159.4	1.79
8	0	-200	800	159.3	1.62
9	-100	-200	800	159.1	6.07
10	100	200	1800	159.4	3.07
11	0	200	1800	159.2	5.32
12	-100	200	1800	159.2	7.12
13	100	0	1800	159.5	0.69
14	0	0	1800	159.3	2.21
15	-100	0	1800	159.2	4.90
16	100	-200	1800	159.5	1.52
17	0	-200	1800	159.4	3.94
18	-100	-200	1800	159.5	5.61
19	100	200	2800	159.7	3.74
20	0	200	2800	159.6	4.62
21	-100	200	2800	159.9	5.66
22	100	0	2800	160.1	1.76
23	0	0	2800	159.8	2.61
24	-100	0	2800	159.8	3.75
25	100	-200	2800	160.0	3.02
26	0	-200	2800	159.9	4.10
27	-100	-200	2800	160.2	4.65

Data presented in Table 4 indicate that within the strapping tape channel, the maximum recorded temperature was 160.2 °C, with an average of 159.4 °C. The resulting maximum temperature difference (ΔT_max) was 1.5 °C, which falls within the process-specific tolerance of ±2 °C.

In contrast, the airflow distribution exhibited significant non-uniformity, attributable to the confined duct geometry. The local velocity reached a maximum of 9.20 m/s against a cross-sectional average of 4.10 m/s. This high variability is quantified by a relative root-mean-square deviation (σ_v) of 0.54.

3.3 Structure Optimisation Scheme Design and Effect Analysis

Given the relatively uniform temperature distribution achieved, the uniformity of the airflow velocity field emerges as the critical factor determining the heating effectiveness of the tape blank. To address the identified flow maldistribution, four distinct optimisation schemes were designed, capitalising on the recognised advantages of flow guide vanes—namely, efficient flow guidance, structural simplicity, and ease of fabrication and installation. Drawing on documented applications of baffles in drying equipment [2,5,11], the proposed schemes are: (1) a curved baffle structure; (2) a combination of curved and vertical baffles; (3) a combination of curved and horizontal baffles; and (4) an integrated structure comprising curved, vertical, and horizontal baffles. These modified configurations are illustrated in Figure 7.

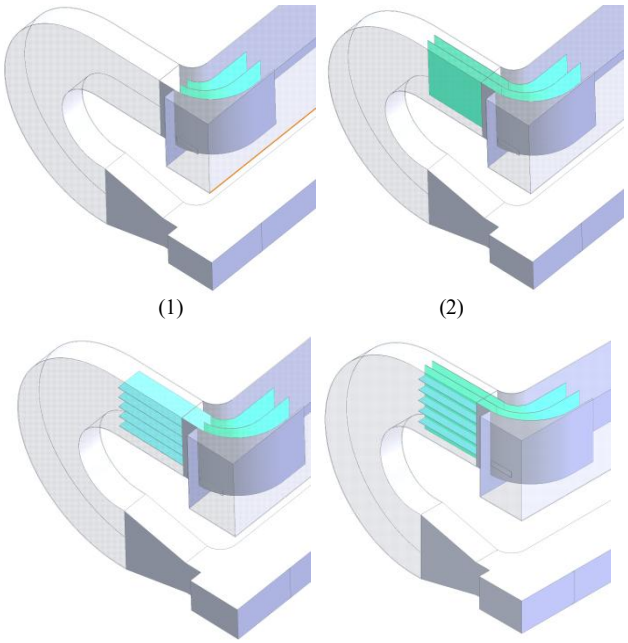

Figure 7: 3D Models of the 4 Optimised Oven Designs

3.3.1 Comparison of optimisation schemes

The results of the heat flow field (Z=800mm) of the strapping tape channel of each scheme are shown in Figure 8, and the performance comparison is shown in Table 5, Scheme 1 has the best optimisation effect.

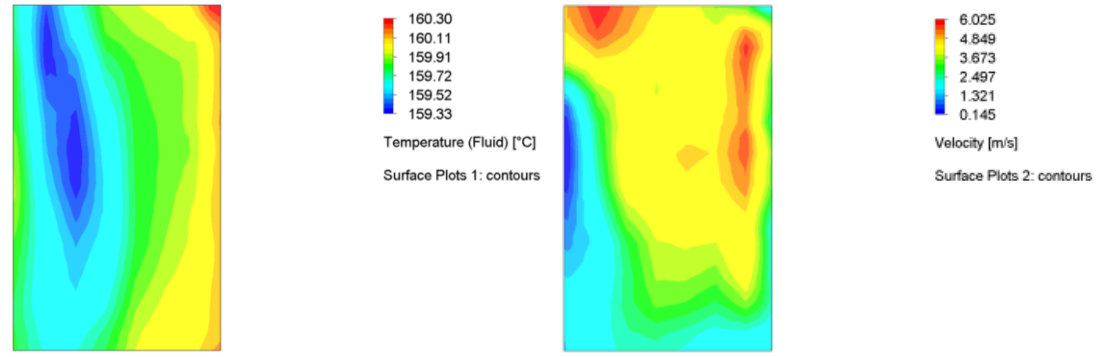

(1)

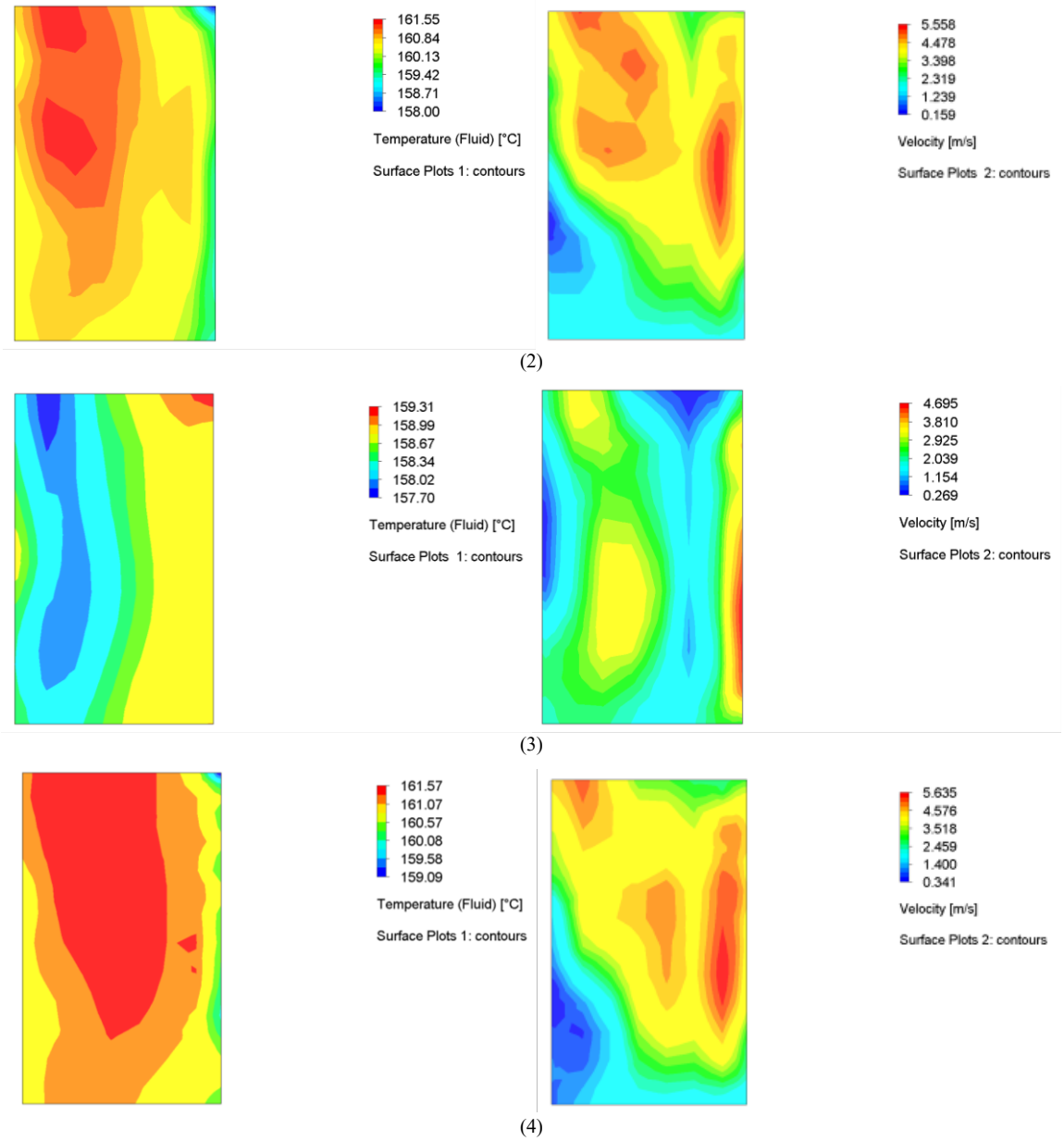

Figure 8: Temperature and velocity diagram at Z=800mm

Table 5: Comparison of the performance of each optimisation scheme

Scheme No.	Maximum temperature difference/°C	Velocity Relative Root Mean Square Difference σ_v
Original structure	1.5	0.54
Scheme 1	1.0	0.25
Scheme 2	4.2	0.23
Scheme 3	3.4	0.25
Scheme 4	3.4	0.25

The comparative results indicate that Scheme 1 (curved baffle only) delivers the most favourable performance. It reduces the maximum temperature difference to 1.0 °C—a 33.3% improvement over the baseline design. Simultaneously, it significantly enhances flow uniformity, lowering the relative RMS deviation (σ_v) to 0.25, which corresponds to a reduction of 53.7%.

While Scheme 2 achieves marginally better flow uniformity (σ_v = 0.23), it induces an excessive temperature difference of 4.2 °C, exceeding the permissible process limit. Schemes 3 and 4 yield moderate temperature differences of 3.4 °C, an improvement over Scheme 2 yet substantially higher than Scheme 1. Their flow uniformity is comparable to that of Scheme 1.

Consequently, Scheme 1 is identified as the optimal design, offering the best practical balance between thermal homogeneity and flow distribution uniformity.

3.4 Engineering Verification of the Optimised Scheme

Scheme 1 was implemented on the strapping tape production line and subjected to a continuous 72-hour stability test. The operational results confirm the scheme's effectiveness: the maximum temperature differential within the oven's strapping channel remained within 2 °C. The produced strapping consistently met all relevant industry standards for mechanical properties. Furthermore, the fluctuation in product width was reduced from the original ±0.3 mm to ±0.2 mm. These outcomes collectively validate the engineering practicality and efficacy of the proposed optimisation.

4. Conclusion

(1) The computational model of the double-belt stretching oven, developed using SolidWorks Flow Simulation, demonstrates good reliability in capturing the distribution characteristics of both the temperature and velocity fields within the oven.

(2) Analysis of the baseline design reveals a significant deficiency in airflow uniformity, characterised by a relative RMS velocity deviation of 0.54 and a maximum temperature difference of 1.5 ℃ in the working zone. This flow maldistribution directly contributed to product width fluctuations of ±0.3 mm in the produced PP strapping.

(3) The incorporation of a curved baffle within the air duct (Scheme 1) proved to be the most effective optimisation. This modification reduced the relative RMS velocity deviation to 0.25 and narrowed the product width fluctuation to ±0.2 mm, representing a 33.3% improvement in dimensional consistency.

(4) The successful implementation and stable operation of this optimised scheme on the production line validates its engineering practicality. It provides a technically viable solution for enhancing the precision of strapping tape stretching ovens and offers a valuable reference for optimising similar thermal processing equipment in plastics manufacturing.

References

[1] Fengqian Zhang, Dali Gao, Lichu Chu, et al. Influence of stretching process on crystalline orientation and tensile strength of polypropylene sheet[J]. Petrochemistry, 2022, 51(11):1289-1293.
[2] SHI Jianfang, WU Zhonghua, LIU Qing, et al. CFD simulation and optimisation of hot air flow field of tunnel drying kiln under different air intake schemes[J]. Journal of Agricultural Engineering, 2014, 30(14): 315-321.
[3] BEDELEAN B. Comparative analysis between a drying kiln designed with and without top baffles[J]. Journal of the Indian Academy of Wood Science, 2014, 11(1): 39-44.
[4] Sjövall F ,Wallin M .Shape and topology optimization for contact applications[J].International Journal of Solids and Structures,2026,328113825-113825.
[5] AMJAD W, MUNIR A, ESPER A, et al. Spatial homogeneity of drying in a batch-type food dryer with diagonal airflow design[J]. Journal of Food Engineering, 2015, 144: 148-155.
[6] Lin, Zhe,Xiao,et al. Optimization of Internal Flow Field and Energy Consumption Reduction Strategies for Quantitative Valves in Packaging Machinery Based on Fluid Mechanics[J]. INTERNATIONAL JOURNAL OF HEAT AND TECHNOLOGY,2025,Vol.43(5): 1809-1816.
[7] Wang FJ. Computational fluid dynamics analysis [M]. Beijing: Tsinghua University Press, 2004: 120-124.
[8] Peng Jun Hu Qideng. SolidWorks Flow Simulation Engineering Examples [M]. Beijing: Mechanical Industry Press, 2024: 19-27.
[9] He WK. Numerical simulation research on wind environment characteristics of high-rise twin-tower complex body building [D]. Hangzhou: Zhejiang University of Technology, 2015: 19-22.
[10] Luo Quanquan, Li Baoguo, Yuan Chenghao. Optimisation study of airflow in drying chamber based on CFD [J]. Packaging and Food Machinery, 2018, 36(5): 27-31.
[11] ZHANG Hong, LIU Jun, WANG Li. Research on temperature field characteristics of forced convection oven and its optimisation[J]. Plastics Industry, 2025, 53(10): 67-71.